Title: A unifying motif for spatial and directional surround suppression

Abbreviated title: Surround suppression in MT

Author names and affiliation: Liu D. Liu[1], Kenneth D. Miller[2], and Christopher C. Pack[1]

[1]Department of Neurology and Neurosurgery, Montreal Neurological Institute, McGill University, Montreal, Quebec H3A 2B4, Canada

[2]Department of Neuroscience, Center for Theoretical Neuroscience, Swartz Program in Theoretical Neuroscience, Kavli Institute for Brain Science, College of Physicians and Surgeons, Columbia University, New York, NY 10032, USA

Corresponding author: Christopher C. Pack;

christopher.pack@mcgill.ca;

Montreal Neurological Institute, Montreal, Quebec H3A 2B4, Canada

Number of pages: 42

Number of figures: 6

Number of words for Abstract, Introduction, and Discussion: 245, 650, and 1487

Conflict of interest: The authors declare no competing financial interests.

Acknowledgements: This work was supported by grants from the Canadian Institutes of Health Research to C.C.P. (PJT-148488) and L.D.L. (CGSD-121719), and NIH R01-EY11001 and the Gatsby Charitable Foundation (K.D.M.). We would like to thank Julie Coursol and the staff of the Animal Care Facility (Montreal Neurological Institute) for excellent technical support.

Abstract

In the visual system, the response to a stimulus in a neuron's receptive field can be modulated by stimulus context, and the strength of these contextual influences vary with stimulus intensity. Recent work has shown how a theoretical model, the stabilized supralinear network (SSN), can account for such modulatory influences, using a small set of computational mechanisms. While the predictions of the SSN have been confirmed in primary visual cortex (V1), its computational principles apply with equal validity to any cortical structure. We have therefore tested the generality of the SSN by examining modulatory influences in the middle temporal area (MT) of the primate visual cortex, using electrophysiological recordings and pharmacological manipulations. We developed a novel stimulus that can be adjusted parametrically to be larger or smaller in the space of all possible motion directions. We found, as predicted by the SSN, that MT neurons integrate across motion directions for low-contrast stimuli, but that they exhibit suppression by the same stimuli when they are high in contrast. These results are analogous to those found in visual cortex when stimulus size is varied in the space domain. We further tested the mechanisms of inhibition using pharmacologically manipulations of inhibitory efficacy. As predicted by the SSN, local manipulation of inhibitory strength altered firing rates, but did not change the strength of surround suppression. These results are consistent with the idea that the SSN can account for modulatory influences along different stimulus dimensions and in different cortical areas.

Significance Statement

Visual neurons are selective for specific stimulus features in a region of visual space known as the receptive field, but can be modulated by stimuli outside of the receptive field. The SSN model has been proposed to account for these and other modulatory influences, and tested in V1. As this model is not specific to any particular stimulus feature or brain region, we wondered whether similar modulatory influences might be observed for other stimulus dimensions and other regions. We tested for specific patterns of modulatory influences in the domain of motion direction, using electrophysiological recordings from MT. Our data confirm the predictions of the SSN in MT, suggesting that the SSN computations might be a generic feature of sensory cortex.

Introduction

Spiking activity is the main mechanism of communication in the nervous system. Electrophysiological recordings provide a means of studying the relationships between spiking activity and sensory stimuli, but they generally do not provide direct insight into the circuits that give rise to these relationships. Such circuits involve an interplay of excitation and inhibition.

Recent work suggests that spiking activity in the visual cortex is modulated by a type of circuit known as the Stabilized Supralinear Network (SSN) (Rubin et al., 2015). The SSN involves recurrent excitation that amplifies weak inputs and inhibition that stabilizes network activity. In V1, one type of modulatory influence is surround suppression, which is a decrease in a neuron's firing rate when the size of a stimulus exceeds that of the receptive field (Allman et al., 1985; Jones et al., 2001; Cavanaugh et al., 2002). Surround suppression is stronger for high-contrast stimuli than for low-contrast stimuli (Sceniak et al., 1999; Pack et al., 2005; Tsui and Pack, 2011).

For low-contrast stimuli, the SSN exhibits weak activation in the receptive field center, while recurrent inputs primarily provide excitation. When the center is strongly activated, recurrent interactions become stronger, and dominated by inhibition. The local network's balance is then tilted towards inhibition, which suppresses both excitatory and inhibitory neurons (Tsodyks et al., 1997; Ozeki et al., 2009). Thus, contrast-dependent surround suppression emerges from the dynamics of recurrent activity, without the need for explicit assumptions about different thresholds for excitation and inhibition (Rubin et al., 2015).

Although the model has been primarily tested with data from V1, the underlying principles are generic (Ozeki et al., 2009; Rubin et al., 2015; Miller, 2016). That is, one should be able to predict the response properties of neurons in other cortical regions based on the

structure of the SSN and the topography of the area from which the recordings are obtained. In particular, if the connection strength between neurons decreases with their distance in a feature space (e.g., preferred orientation in V1, (Cossell et al., 2015); or preferred direction in MT), then the SSN model predicts that there should be contrast-dependent surround suppression in that feature space, just as in retinotopic space (Rubin et al., 2015). Area MT provides a straightforward means of testing the genericity of the SSN: MT contains a local columnar structure based on selectivity for visual motion (Albright, 1984), so that nearby neurons encode similar motion directions (Born and Bradley, 2005). The SSN therefore makes the prediction, by analogy with V1 surround suppression, that MT firing rates should be decreased when stimuli activate MT neurons with a wider range of motion preferences. Furthermore, in the SSN model, such intracortical interactions vary with the overall level of activation, so that direction-domain suppression should be stronger at higher contrasts. Finally, a counterintuitive aspect of the SSN is that the strength of suppressive interactions are changed little by local blockade of GABAergic inputs (Ozeki et al., 2004; Ozeki et al., 2009), because the suppression is caused by a withdrawal of excitatory input that is not disrupted by local manipulations of inhibition.

We tested these ideas by designing a stimulus that could be manipulated parametrically to be larger or smaller in the space of directions, while maintaining a fixed size in visual space. We found that responses in MT were indeed suppressed by stimuli with a wider range of motion directions, but only when the stimulus was high in contrast. At low contrast, neurons integrated over a larger spread of motion directions, as has been observed for spatial integration (Levitt and Lund, 1997; Kapadia et al., 1999; Sceniak et al., 1999). This provided support for a key prediction of the SSN. In addition, we confirmed a counterintuitive property of the SSN, namely that blockage of GABAergic inhibition does not reduce neuronal surround suppression. These

results are consistent with the idea that the SSN is a generic mechanism of cortical computation (Miller, 2016).

Materials and Methods

Electrophysiological Recordings and Visual Stimuli

Two adult female rhesus monkeys (*Macaca mulatta*, both 7 kg) were used for electrophysiological recordings in this study. Before training, under general anesthesia, an MRI-compatible titanium head post was attached to each monkey's skull. The head posts served to stabilize their heads during subsequent training and experimental sessions. For both monkeys, eye movements were monitored with an EyeLink1000 infrared eye tracking system (SR Research) with a sampling rate of 1,000 Hz. All procedures conformed to regulations established by the Canadian Council on Animal Care and were approved by the Institutional Animal Care Committee of the Montreal Neurological Institute.

Area MT was identified based on an anatomical MRI scan, as well as depth, prevalence of direction-selective neurons, receptive field size to eccentricity relationship, and white matter to grey matter transition from a dorsal-posterior approach. We recorded single units using linear microelectrode arrays (V-Probe, Plexon) with 16 contacts.

Neural signals were thresholded online, and spikes were assigned to single units by a template-matching algorithm (Plexon MAP System). Offline, spikes were manually sorted using a combination of automated template matching, visual inspection of waveform, clustering in the space defined by the principle components, and absolute refractory period (1 ms) violations (Plexon Offline Sorter).

Visual motion stimuli were displayed at 60 Hz at a resolution of 1,280 by 800 pixels; the viewing area subtended 60° × 40° at a viewing distance of 50 cm. Stimuli consisted of random dot stimuli displayed on a gray background (luminance of 98.8 cd/m^2). Half the dots were black, and half the dots were white, resulting in a constant mean luminance across stimulus conditions.

At 100% contrast, the black dots had luminance of 0.4 cd/m^2, and the white dots had luminance of 198 cd/m^2. The intermediate contrasts were defined as a percentage of the luminance difference from the gray background luminance, contrast = |(luminance - 98.8 cd/m^2) / 98.8 cd/m^2|. Animals were trained to fixate on a small dot at the center of the screen. Stimuli were shown after 300 ms of fixation. Each stimulus was presented for 500 ms, and the animals were required to maintain fixation throughout the stimulus and for another 300 ms after the end of the stimulus to receive a liquid reward. In all trials, gaze was required to remain within 2º of the fixation point in order for the reward to be dispensed. Data from trials with broken fixation were discarded.

The direction tuning and contrast response of the single units were quantified using 100% coherent dot patches placed inside the receptive fields. Offline the receptive field locations were further quantified by fitting a spatial Gaussian to the neuronal response measured over a 5 x 5 grid of stimulus positions. The grid consisted of moving dot patches centered on the initially hand-mapped receptive field locations. We confirmed that all neurons included in our analysis had receptive field centers within the stimulus patch used.

Size Tuning Stimuli in Direction Space

We designed a stimulus that would allow us to study surround suppression in the motion domain in a manner that was analogous to studies in the spatial domain. In this conception, the input to the receptive field "center" is the strength of motion in a range about the neuron's preferred direction. The "surround" is then motion in other directions, and the bandwidth of the center plus surround is the size of the stimulus in direction space. That is, a stimulus that contains motion in a range of directions spanning 180° is larger than a stimulus that spans a range of 60°. For these

experiments we did not manipulate the spatial size of the stimulus, but rather fixed it according to the size of the hand-mapped spatial receptive field.

Our stimuli made use of random dots, each of which could be assigned to either a noise or a signal pool. The noise dots moved in random directions. The signal dots moved in a range of directions that straddled the preferred direction of each neuron. All dots moved at the same fixed speed of 8 or 16º/s, depending on the speed preference of the neuron. In all cases, dot patches were centered on the receptive fields determined by hand mapping. All conditions were interleaved randomly, and each stimulus was repeated 20 times.

We wished to change the size of the stimulus in direction space without changing other stimulus variables to which the neurons were sensitive. However, changing the size in direction space entails changing other low-level stimulus parameters (e.g., total number of dots or total amount of motion energy), which could confound our interpretation of the data. We therefore used two different methods to vary the stimulus bandwidth in direction space, each of which entailed changing a different low-level aspect of the stimulus.

In the first method, we kept the total number of stimulus dots fixed, and increased the motion bandwidth by drawing dots from a noise pool. Thus the total number of dots was identical for all stimuli, across variations in direction bandwidth. We constructed stimuli that contained signal dots moving in 1, 2, 3, and 4 directions, and each increase in the number of motion directions involved recruiting 25% of the noise dots to move coherently in the new direction (Fig. 2A). For the 1-direction stimulus, 25% of the dots moved in the neuron's preferred direction, and 75% of the noise dots moved in random directions. For the 2-direction stimulus, we took 25% of the total number of dots and assigned them motion directions in equal numbers to 30° clockwise and counterclockwise from the preferred direction; to keep the total

166 number of dots constant we decreased the number of noise dots accordingly. This gives a
167 stimulus direction bandwidth of 60º (Fig. 2B). Similarly, for stimuli with 3 and 4 signal
168 directions, the noise dots pool was 25% and 0%, and the additional 25% of dots moved in
169 directions +/-60° and +/-90° from the preferred direction. This gives a stimulus direction
170 bandwidth of 120º and 180º, respectively (Fig. 2B). This paradigm thus allowed us to test the
171 influence of size in direction space for stimuli comprised of a fixed number of dots and a fixed
172 amount of overall motion energy.

173 However, in this approach, increases in motion bandwidth are yoked to decreases in
174 noise, which might be expected to affect the strength of inhibitory inputs on their own (Hunter
175 and Born, 2011). Thus, we also tested neurons using a second method, in which there was no
176 noise pool, and we increased the size in direction space by simply adding more dots that moved
177 in different directions. In this case the center stimulus strength (i.e. the strength of motion in the
178 preferred direction) was constant across conditions, but the total number of dots (and hence the
179 total motion energy) increased with stimulus size. The lowest dot density used was 2
180 dots/degree^2, which is beyond the density at which MT responses typically saturate, at least for
181 100% coherence stimuli (Snowden et al., 1992).

182 We again tested four different direction conditions (Fig. 3A). As before, stimuli with one
183 direction contained signal dots that all moved in the neuron's preferred direction, and dot density
184 was 2 dots/degree^2. For stimuli containing more signal directions, additional dots were added,
185 and these moved at 30° clockwise and counterclockwise from the preferred direction, raising the
186 dot density to 4 dots/degree^2. Similarly, for stimuli with 3 and 4 signal directions, the dot density
187 was 6 dots/degree^2 and 8 dots/degree^2, with additional directions being added at 30° increments.

188 For all size tuning experiments in direction space, we tested each of the 4 sizes at high
189 and low contrasts. High contrast was defined as 100% contrast, and the low contrast was chosen
190 online to be around the c_{50} of the contrast response function obtained with the 100% coherent dot
191 patch. Offline, we eliminated neurons for which the response at any tested contrast was below 2
192 standard deviations of the spontaneous baseline firing rate.
193
194 *Grating, plaid, and pattern selectivity*
195 We tested a subset of MT neurons (n = 65) with a standard measure of motion integration, the
196 plaid stimulus (Movshon et al., 1985). Direction selectivity for each neuron was first measured
197 with a 100% contrast drifting sinusoidal grating of spatial frequency of 0.5 cycles/º. Stimulus
198 size and temporal frequency were matched to the neuron's preferences. Plaid stimuli were
199 constructed by superimposing two gratings (Fig. 4A).
200 We used the standard approach to quantify the component and pattern selectivity of each
201 neuron (Smith et al., 2005). The partial correlations for the pattern and component predictions
202 were calculated as,

203 $$PC_p = \frac{r_p - r_c r_{pc}}{\sqrt{(1 - r_c^2)(1 - r_{pc}^2)}}$$

204 $$PC_c = \frac{r_c - r_p r_{pc}}{\sqrt{(1 - r_p^2)(1 - r_{pc}^2)}}$$

205 Where r_p and r_c are the correlations between the plaid response and the pattern and component
206 predictions, respectively, and r_{pc} is the correlation between the pattern and component
207 predictions. The partial correlations are z-scored as,

208 $$Z_p = 0.5ln\left(\frac{(1 + PC_p)/(1 - PC_p)}{\sqrt{1/(n-3)}}\right)$$

209 $$Z_c = 0.5ln\left(\frac{(1+PC_c)/(1-PC_c)}{\sqrt{1/(n-3)}}\right)$$

210 Where n = 12 is the number of directions. The pattern index was calculated as $Z_p - Z_c$.

211

212 *Pharmacological Injections*

213 The pharmacological injection system has been previously described (Liu and Pack, 2017).
214 Briefly, our linear electrode arrays contained a glass capillary with an inner diameter of 40 µm.
215 One end of the capillary was positioned at the opening between contacts 5 and 6 of the array
216 (contact 1 was most dorsal-posterior). The other end of the capillary was connected via plastic
217 tubing to a Hamilton syringe for the injection of pharmacological agents with a minipump.

218 To effectively manipulate neuronal responses without compromising isolation, we
219 typically used injections of 0.1-0.2 µL at 0.05 µL/min. For GABA, we used a concentration of
220 25 mM, which reduced neural activity without silencing it completely (Bolz and Gilbert, 1986;
221 Nealey and Maunsell, 1994). For gabazine, the concentration was 0.05 mM, and we used
222 injections of approximately 0.5 µL at 0.05 µL/min. In a few cases, this induced unstable and
223 synchronized responses in the nearby neurons (Chagnac-Amitai and Connors, 1989). The
224 electrophysiological recordings in those sessions were not further analyzed here.

225

226 *Data Analysis*

227 MT direction tuning curves $r(x_d)$ were characterized by fitting a Gaussian function to the mean
228 responses using the least-squares minimization algorithm (lsqcurvefit in MATLAB). The
229 Gaussian function is

230 $$r(x_d) = ae^{-0.5d(\theta,\, x_d)^2/b^2} + m$$

where a scales the height of the tuning curve; b determines the tuning curve width; x_d is the motion direction; θ is the preferred direction of motion; and m is the baseline firing rate of the cell. $d(\theta, x_d)$ is the shortest distance around the 360 degree circle between θ and x_d.

The contrast response functions $r(x_c)$ were fitted with a Naka-Rushton function,

$$r(x_c) = R_{max}\frac{x_c^n}{x_c^n + c_{50}^n} + m$$

where R_{max} scales the height of the contrast response function; n determines the slope; c_{50} is the contrast at which the response function achieves half of its maximum response; and m is the baseline firing rate of the cell. x_c is the contrast.

The neuronal size tuning curves $r(x_s)$ in retinotopic space were fitted by a Difference of Error functions (DoE) (Sceniak et al., 1999; DeAngelis and Uka, 2003),

$$r(x_s) = A_e erf\left(\frac{x_s}{s_e}\right) - A_i erf\left(\frac{x_s}{s_e + s_i}\right) + m$$

where A_e and A_i scale the height of the excitatory center and inhibitory surround, respectively. s_e and s_i are the excitatory and inhibitory sizes, and m is the baseline firing rate of the cell. x_s is the stimulus size.

The size suppression index (SI_S) for each neuronal size tuning curve was calculated as $SI_S = (R_m - R_L)/R_m$, where R_m is the maximum across responses to different stimulus sizes and R_L is the response observed at the largest size. Since using the raw responses is sensitive to noise at both the maximum response and the response at the largest size, we used the values from the DoE fits for SI calculations.

Since we only measured the response at 4 sizes in the directional space, we were unable to fit a DoE function to the directional size tuning curves. Instead, to capture potential suppressive influences in the direction domain, we calculated a direction integration index from

the raw data $II_D = (R_L - R_S) / (R_L + R_S)$, where R_L is the response observed at the largest size and R_S is the response observed at the smallest size.

SSN Model Simulations

We first simulated a 1D ring model, which captures putative interactions among neurons representing different motion directions (Fig. 1A). Details of this model can be found elsewhere (Rubin et al., 2015). Our model differs in that the ring is 360 degrees in extent (vs. 180 degrees in Rubin et al., 2015), representing all possible motion directions. There is an excitatory (E) and inhibitory (I) neuron at every integer position $x_i = 0^o, 1^o, \ldots, 359^o$, where x_i represents the preferred direction of the corresponding E and I cells. We can write the model equation in matrix notation as,

$$\tau \frac{d}{dt}\boldsymbol{r}(x_i) = -\boldsymbol{r}(x_i) + k([\boldsymbol{W}*\boldsymbol{r}(x_i) + c\boldsymbol{h}(x_i)]_+)^n$$

where $\boldsymbol{r}(x_i)$ is the vector of firing rates of the excitatory and inhibitory neurons with preferred motion direction x_i, $\boldsymbol{W}(y)$ is the weight matrix of E → E, E → I, I → E, and I → I connections between neurons separated by angular distance y (measured as shortest distance around the 360 degree circle). The connections $W_{ab}(y) = J_{ab}G\sigma_{dir}(y)$, where $J_{EE} = 0.44$, $J_{EI} = 0.23$, $J_{IE} = 0.042$, $J_{II} = 0.018$, $G\sigma_{dir}(y)$ is a Gaussian function with standard deviation of 64º. $\boldsymbol{W}*\boldsymbol{r}(x_i)$ is the convolution $\sum_j \boldsymbol{W}(x_i\text{-}x_j)\boldsymbol{r}(x_j)$ where the sum is over all preferred directions x_j , $\boldsymbol{h}(x_i)$ is the vector of external input to the E and I neurons preferring x_i, and c is the strength (monotonically related to contrast) of the input. The elements of the vector of input to the neuron, $\boldsymbol{W}*\boldsymbol{r}(x_i) + c\boldsymbol{h}(x_i)$, are thresholded at zero before being raised to the power n: $[z]_+ = 0 \; if \; \boldsymbol{z} < 0, = z \; if \; z \geq 0$ (the operations of thresholding and raising to a power are applied separately to each element of the vector). k and n are identical for E and I neurons, with k

276 = 0.04 and $n = 2$. τ is a diagonal matrix of the time constant for E cells, $\tau_E = 20$ ms, and for I
277 cells, $\tau_I = 10$ ms.
278 We simulated network responses to random dot field stimuli of variable coherence. We
279 assumed that a coherent dot stimulus of a given direction gives input to MT neurons proportional
280 to a Gaussian function, of standard deviation 60º, of the difference (shortest distance around a
281 360º circle) between the neuron's preferred direction and the stimulus direction. The non-
282 coherent (noise) dots gave equal input, proportional to 1/360, to neurons of all preferred
283 directions. The strength of the stimulus is given by a parameter *c*, identified as the "contrast" in
284 Figure 1. As in our electrophysiological experiments, we used stimuli corresponding to 4
285 different sizes in direction space (Fig. 2A). Thus for the smallest size, 25% of the input, $\boldsymbol{h}$, was
286 modelled as a Gaussian distribution around the preferred direction (peak of the Gaussian = $c/4$),
287 while the remaining 75% was spread equally around the ring (uniform distribution of size $(3/4) \times$
288 $c/360$). At 2 directions, an additional 25% was taken from the non-coherent input and added to
289 Gaussian spreads about +/-30° from the preferred direction (these two Gaussians have peak =
290 $c/8$; noise amplitude becomes $(1/2) \times c/360$). 3 and 4 directions followed in a similar manner
291 while the total input strength was kept constant across sizes. We also simulated the same set of
292 stimuli except without a noise background (so that the total input strength grew with increasing
293 number of directions), and the results were qualitatively similar as presented in Results.
294
295 *Experimental design and statistical analysis*
296 We used two female rhesus monkeys (*Macaca mulatta*) for electrophysiological recordings in
297 this study; this is standard for electrophysiological studies involving monkeys. We used the
298 Wilcoxon rank-sum test to evaluate the difference between the Integration Index at low and high

contrast, and the difference between Direction Tuning Width and Suppression Index before and after injection of Gabazine. We calculated Pearson correlation coefficients to evaluate the relationship between the Pattern Index and Direction Tuning Width with the Integration Index. We used built-in MATLAB functions and custom scripts to perform the analyses. The complete results of the statistical analyses for each experiment can be found in the corresponding Results section.

305 **Results**

306 In this section, we first present simulation results for the SSN. We then test a crucial model
307 prediction with neurophysiological recordings from MT neurons in awake and behaving
308 macaques. The theoretical and empirical results show that surround suppression in the motion
309 domain behaves similarly to surround suppression in the space domain, with integration at low
310 contrasts switching to suppression at high contrasts (Figs. 2 and 3). We also find that pattern-
311 selective cells (as assayed from plaid responses) show greater motion integration than
312 component-selective cells (Fig. 4). Finally, as predicted by the SSN model, local
313 pharmacological manipulation of inhibition does not alter spatial surround suppression, although
314 our methods had the expected effects on directional tuning width (we did not examine effects on
315 surround suppression in the direction domain) (Figs. 5 and 6).

316

317 *Stabilized supralinear network predicts contrast-dependent surround suppression in the*
318 *direction domain in MT*

319 Previous instantiations of the SSN have considered a model in which connections are defined
320 either across a retinotopic sheet of the kind found in V1 or across a ring of preferred orientations
321 (Ahmadian et al., 2013; Rubin et al., 2015; Miller, 2016). Like orientation, motion direction is a
322 circular variable, but it takes values over 360° rather than 180° as for orientation. Thus to
323 examine the properties of the SSN in this circular space, we first simulated a ring model ((Rubin
324 et al., 2015); Fig. 1A) of motion direction space. This represents neurons of varying preferred
325 directions sharing a common location in retinotopic space.

326 In general, the SSN predicts that contrast-dependent surround suppression should occur
327 in any stimulus feature dimension, provided certain minimal connectivity conditions are met, e.g.

328 average connection strength between neurons decreases with the dimensional distance between
329 them. We accordingly assumed that the strengths of connections between neurons on the ring
330 decreased with increasing difference in their preferred directions. By analogy with the study of
331 size-tuning in the spatial domain, we tested the SSN with stimuli of different motion-domain
332 sizes. We increased the size of the stimulus in direction space by including stimuli at
333 increasingly wider ranges of directions about the preferred direction (the "center" of the
334 receptive field). As described in Methods, we considered size or bandwidth 0º (preferred-
335 direction stimulus only), 60º (adding stimuli at +/- 30º about the preferred), 120º (adding
336 additional stimuli at +/- 60º), and 180º (additional stimuli at +/- 90º). For each motion size, we
337 examined different levels of stimulus contrast, represented as scaling the strengths of all inputs.
338 The simulation results (Fig. 1B) show that the model predicts strong direction-domain
339 surround suppression at high contrast, but not at low contrast. Specifically, at low contrasts (red),
340 increasing the range of motion directions leads to increased responses with a hint of suppression
341 for the largest stimulus size, while at high contrasts larger motion-domain stimulus sizes lead to
342 strong suppression (blue). Intermediate contrasts give an intermediate result (black). These
343 results change very little with changes in the total number of dots in the stimulus (Fig. 1C), a
344 factor that we consider in our experiments below (Fig. 3). Thus the model consistently predicts
345 direction-domain suppression that is analogous to space-domain surround suppression. In the
346 SSN, the dependence of surround suppression on contrast arises generically from the dynamics
347 of the SSN in summing inputs, rather than by the assumption of a higher contrast threshold for
348 inhibition, as in previous models (Somers et al., 1998; Huang et al., 2008; Schwabe et al., 2010;
349 Carandini and Heeger, 2012).
350

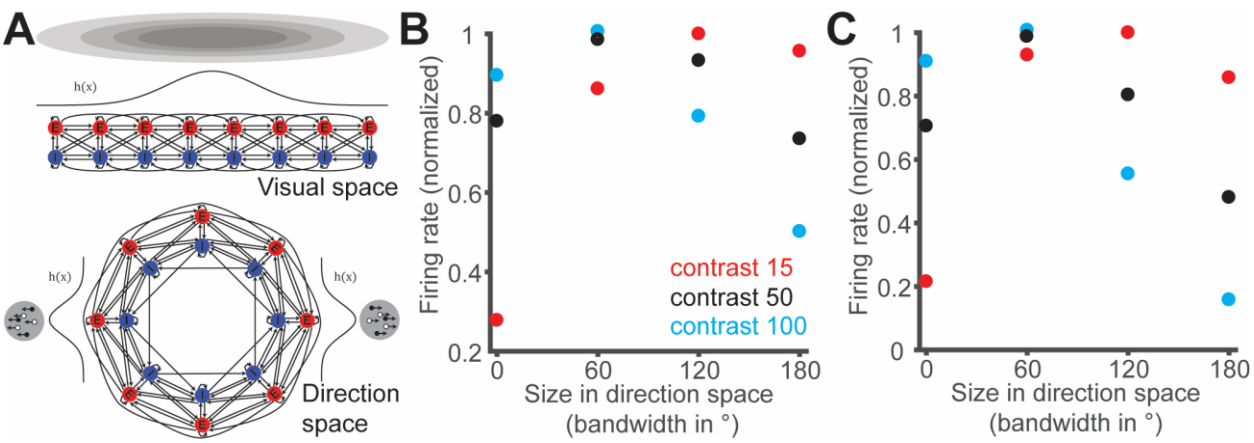

Figure 1. Stabilized supralinear network can account for surround suppression in both spatial and direction domains. **A,** Schematic of the 1D SSN ring model as a direction space analogue of the visual space model. In the visual space model (top), stimuli of different sizes in visual space (gray circles) are simulated as input, *h(x)*, of varying width, to a linear 1D grid of excitatory (E, red) and inhibitory (I, blue) units. The grid positions represent visual space positions. In the direction space (bottom), there are 360 E and I units, with coordinates on the ring as preferred directions. A dot stimulus, *h(x)*, moving at a single direction is a Gaussian-shaped input with standard deviation of 60º. Stimuli including multiple directions simply add such input for each direction. We considered two methods of adding directions: including a "noise pool" stimulus of equal input to all directions, and subtracting from the noise pool as we added directions to keep total input strength unchanged (Fig. 2A); or simply adding additional input as we added directions, without a noise pool (Fig. 3A). **B,** Directional surround suppression at high contrast, but not at low contrast, arises from the dynamics of the model. This simulation result is for the first method of taking dots from a noise pool to add further directions about the preferred (Fig. 2A). The response at each contrast is normalized to the peak response. **C,** The simulation result for the second method of adding dots to further directions about the preferred without a noise pool (Fig. 3A). The response at each contrast is normalized to the peak response.

369

370 *Surround suppression in direction domain of MT*

371 We tested the model predictions by recording from individual MT neurons, using the same
372 stimuli as in the simulations. We first show results for the first type of stimulus described above,
373 in which there was a noise pool of dots moving in random directions. For each neuron we fixed
374 the physical size of each stimulus according to an estimate of the classical receptive field size.
375 We then varied stimulus size in the motion domain, as well as dot contrast. Thus for the smallest
376 stimulus, all the coherent dots moved in the preferred direction of the neuron (Fig. 2A, left), with
377 the remaining dots in the noise pool moving in random directions. To increase the size of stimuli
378 in the motion space, we recruited dots from the noise pool and added them to directions around
379 the preferred direction (Fig. 2A). This manipulation kept the total motion energy and dot density
380 of the stimulus constant across sizes.

381 Figure 2B shows the firing rate of an example MT neuron for stimuli of different
382 contrasts and motion sizes. For the low contrast stimulus (red), firing rate increased with motion
383 size, while for higher contrasts (blue, black) firing rate decreased with motion size. Thus the
384 pattern of firing rates for this neuron was consistent with the SSN prediction that MT neurons
385 would shift from motion-domain integration to suppression as the stimulus contrast was
386 increased (Fig. 1B). Indeed, just as in the space domain, for large stimuli it is possible to increase
387 firing rates by lowering contrast (Fig. 2B; Pack et al., 2005).

388 To examine these effects across the MT population, we calculated the directional
389 integration index (II_D, the difference between responses to the largest and smallest sizes divided
390 by the sum of these responses; see Methods) for data of the kind shown in Figure 2B for 125
391 neurons. The II_D captures the integration of signals across motion directions, with larger II_D

392 values indicating more integration. Across the population (Fig. 2C) the II_D was frequently below
393 zero, indicating a suppression of the response when dots activated the directional surround.
394 Overall the II_D was significantly decreased at high contrast compared to low contrast, consistent
395 with reduced integration at high contrasts ($p < 0.001$, rank sum test). Note that this is not due to a
396 failure of the low contrast stimuli to elicit a response from the neurons, as all neurons except one
397 showed responses to the lowest contrast tested that were significantly above baseline. The one
398 neuron that failed to meet this criterion was eliminated from further analysis. Overall, these
399 results are similar to previous results in the space domain in MT (Pack et al., 2005; Tsui and
400 Pack, 2011). However, the mechanisms of spatial and directional integration for a given cell
401 appeared to be independent, as there was no correlation between the degree of spatial surround
402 suppression and directional surround suppression measured at high contrast in the same neurons
403 (Pearson's $r = -0.06$, $p = 0.46$, N = 124).

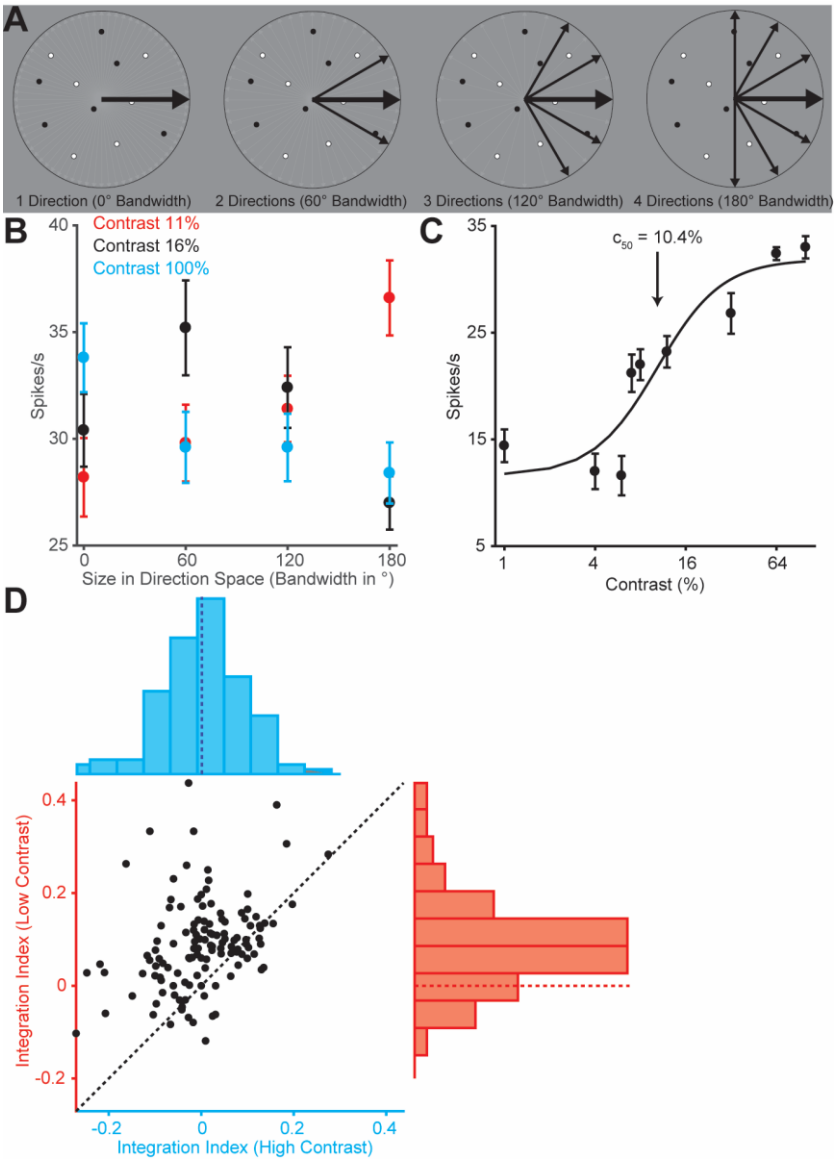

Figure 2. Surround integration and suppression in the direction domain. **A,** Illustration of the stimulus that engages directional surround suppression in MT while the dot density is fixed. **B,** Surround suppression occurs in direction space at high contrast, but not at low contrast for an example neuron. **C,** Contrast response function for the same example neuron using 100% coherent dots in the preferred direction. The line indicates the Naka-Rushton function fit. **D,** Population data for direction surround integration. Scatter plot of the integration index, II_D, at low contrast against the II_D at high contrast (rank sum test, $p < 0.001$). The marginal distributions

412 are histograms of the II_D (Median at low contrast = -0.003; Median at high contrast = 0.051).
413 Dashed lines in the histograms show location of $II_D = 0$.
414
415 We also tested 46 neurons using a second stimulus in which there was no noise pool, and
416 we increased the total number of stimulus dots with size in the direction domain (Fig. 3A). This
417 stimulus was designed to control for a potential confound in the previous experiment, which kept
418 the total number of dots constant across stimulus size. In the latter configuration, increases in
419 direction-domain size were yoked to decreases in the number of noise dots, and because noise
420 includes motion in all directions, this can be viewed as reduction in the strength of the directional
421 surround, analogous to the far surround in retinal space (Angelucci and Bullier, 2003; Angelucci
422 and Bressloff, 2006). The new stimulus was directly analogous to that typically used in size
423 tuning experiments, in which the stimulus is simply expanded to probe the influence of the
424 surround.
425 We tested this subpopulation of MT neurons with both stimuli, and the results are shown
426 in Figures 3B and 3C. For the control stimulus, the II_D is still significantly higher at low contrast
427 than at high contrast (Fig. 3B; $p = 0.04$, rank sum test). Thus integration across direction space
428 was greater at low contrast, regardless of how size was manipulated. For these neurons, we also
429 replicated the previous result using the stimulus with a constant total number of dots (Fig. 3C; p
430 < 0.001, rank sum test). The contrast modulation of II_D was not significantly different for the two
431 stimulus types (rank sum test, $p = 0.45$).
432

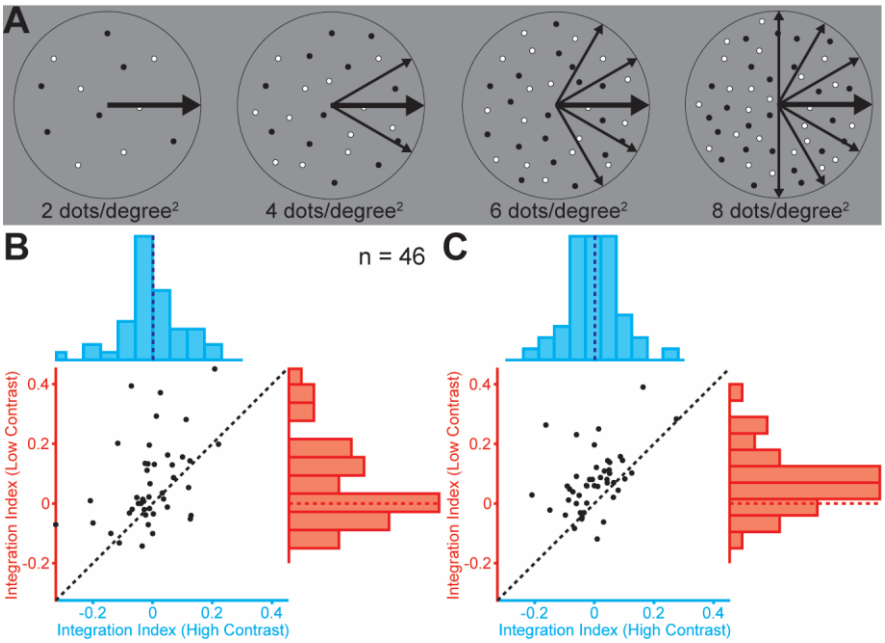

Figure 3. Additional controls for direction surround integration and suppression. **A,** Illustration of the stimulus that engages directional surround suppression in MT while the dot density increases with directional size. **B,** Population data for direction surround integration. Scatter plot of the directional integration index (II_D) at low contrast against the SI at high contrast (rank sum test, $p = 0.04$). The marginal distributions are histograms of the II_D (Median at low contrast = -0.012; Median at high contrast = 0.018). Dashed lines in the histograms show location of $II_D = 0$. **C,** The contrast modulation of II_D for the same 46 neurons as in B, when the number of dots is held fixed by drawing from a noise pool (as in Fig. 2). The conventions are the same as in panel B (Median at low contrast = 0.003; Median at high contrast = 0.065).

Of the complete MT population, 65 were also tested with a standard probe of direction-domain integration, the plaid stimulus (Movshon et al., 1985). Our plaid stimuli consisted of two superimposed sine-wave gratings, moving in directions separated by 120° (Fig. 4A); stimulus size was again matched to the classical receptive field, and contrast was 100%. From the

448 resulting data we computed a pattern index (see Methods; Smith et al., 2005), which captures the
449 extent to which MT neurons integrate the two motion directions; higher values indicate greater
450 integration (Fig. 4B and C). We found that the pattern index was significantly correlated with the
451 directional II_D, as measured in our direction-size-tuning experiments at both low (Fig. 4D;
452 Pearson's $r = 0.33$, $p = 0.01$) and high contrasts ($r = 0.27$, $p = 0.03$). That is, cells with higher
453 pattern indices showed less surround suppression in direction space – greater motion integration
454 -- both at low and high stimulus contrasts. This suggests that area MT might use similar
455 mechanisms to integrate motion signals for dot stimuli and grating stimuli. We also found that
456 there was no correlation between the directional motion integration index and the width of the
457 direction tuning curve, as measured using responses to standard stimuli of drifting dots moving
458 coherently in a single direction (Fig. 4E; Pearson's $r = -0.08$, $p = 0.38$ for low contrast, $r = 0.05$,
459 $p = 0.57$ for high contrast).

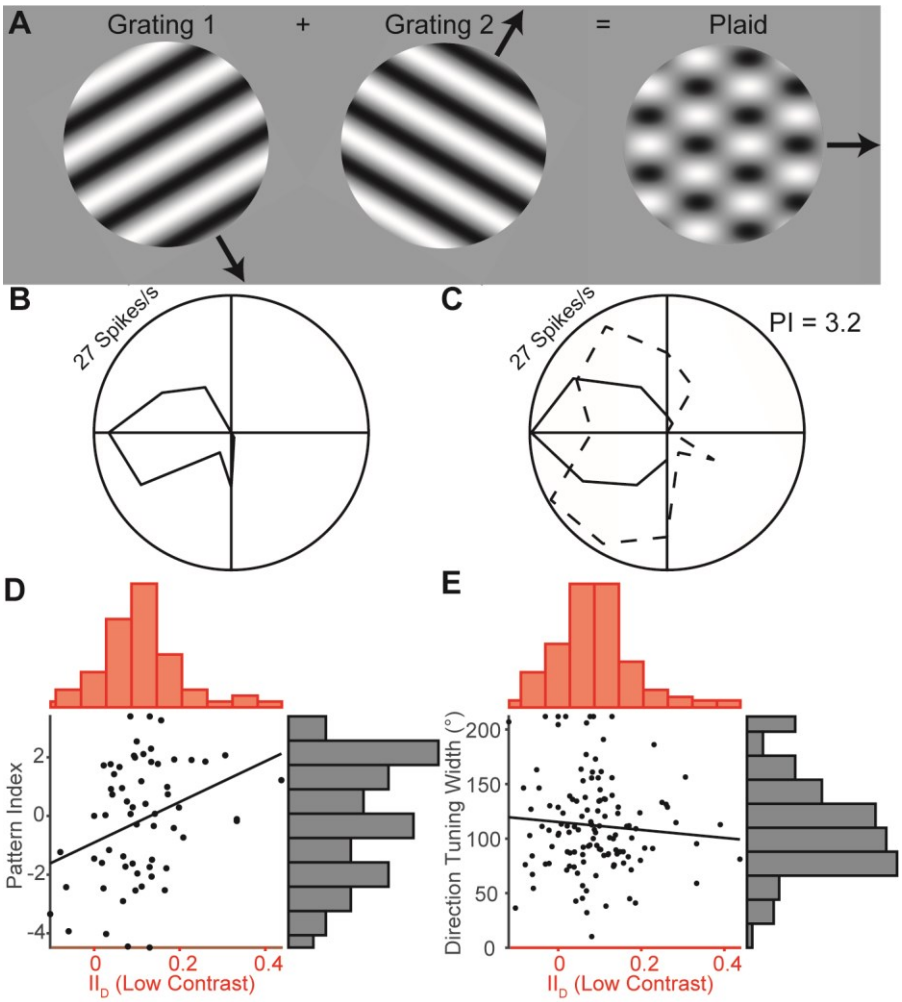

Figure 4. Direction integration with plaid stimuli. **A,** Illustration of the grating (left) and plaid stimuli (right). **B,** Direction tuning curve for an example neuron in response to drifting gratings. **C,** Direction tuning curve for the same neuron in response to moving plaids. The dashed line indicates the component prediction, which is the expected result if the neuron fails to integrate the motion of the plaid. **D,** Population data for motion integration. Scatter plot of the pattern index against the directional integration index (II_D) at low contrast ($r = 0.33$, $p = 0.01$). **E,** Scatter plot of the direction tuning width against the directional integration index (II_D) at high contrast ($r = -0.08$, $p = 0.38$).

470 *GABAergic influence on neuronal direction tuning and surround suppression in the spatial*
471 *domain*
472 Another prediction of the SSN is that local changes in the strength of inhibition should have little
473 or no effect on surround suppression, because surround suppression is a result of withdrawal of
474 network excitation (as well as inhibition), and a local blockade of inhibition will not change
475 these network dynamics (Ozeki et al., 2009). This is different from conventional models, which
476 posit that suppression is induced by an increase in the inhibition that a cell receives, so that a
477 reduction in the inhibition to a given neuron will reduce its surround suppression (Tsui and Pack,
478 2011). Previous work has confirmed the SSN predictions in anesthetized cat V1, using
479 iontophoretic injection of GABA antagonists: inhibitory blockade did not reduce surround
480 suppression (Ozeki et al., 2004). In this section, we examine the effects of pharmacological
481 manipulation of GABA in MT of awake monkeys.
482 We first confirmed that gabazine, a $GABA_A$ receptor antagonist, robustly modulated
483 neuronal firing in MT (Thiele et al., 2012). We measured direction tuning using random-dot
484 stimuli of fixed spatial size, with all dots moving coherently in a single direction (Fig. 5A). We
485 found that injection of gabazine non-specifically increased firing rates across all directions (Fig.
486 5C), leading to increases in direction tuning width, as found previously (Thiele et al., 2004;
487 Thiele et al., 2012). In contrast, injections of GABA decreased firing rates across all directions
488 (Fig. 5E), leading to narrower tuning (Leventhal et al., 2003). Figure 6A summarizes the
489 influence of gabazine on direction tuning widths for a population of 38 MT cells: Tuning width
490 significantly increased following the injection (rank sum test, $p = 0.04$). We did not have enough
491 data from the GABA experiments to perform statistical analyses, but in all 5 experiments,

492 direction tuning width decreased following injection. Overall these results show that local
493 manipulations of GABA concentration had the expected effects on direction tuning in MT.
494 To test the influence of GABA concentrations on surround suppression, we performed
495 standard (space-domain) measurements of size tuning, using random-dot stimuli (100%
496 coherence) of different physical extents, with all dots moving in the neuron's preferred direction
497 (Fig. 5B). Previous work has shown that these stimuli elicit surround suppression in the upper
498 and lower layers in MT, but not in layer 4, suggesting that the suppression is generated through
499 intrinsic connections within MT (Born and Tootell, 1992; Raiguel et al., 1995). This property
500 makes such stimuli useful for testing the predicted role of inhibitory inputs in the SSN.
501 Figure 5D shows size tuning curves from the same MT neuron as in Figure 5C. The pre-
502 injection data (black line) show that the neuron exhibited substantial surround suppression, as the
503 response was reduced significantly with increasing stimulus size. As for the direction tuning
504 curve, injection of gabazine increased firing rates in a non-specific manner. However, in this
505 neuron there was no apparent reduction in surround suppression (Fig. 5D), and this result was
506 generally true for the MT population (n = 38): The size suppression index (SI_S), defined as the
507 difference between the peak response and the response to the largest stimulus divided by the
508 peak response, was similar before and after injection of gabazine (Fig. 6B; rank sum test, p =
509 0.98). These results are similar to those found in V1 of anesthetized cats (Ozeki et al., 2004),
510 despite the much larger volume of gabazine used here. In a smaller sample (n = 5), we found that
511 injection of GABA did not increase surround suppression, despite a strong overall reduction in
512 firing rate (Fig. 5F).

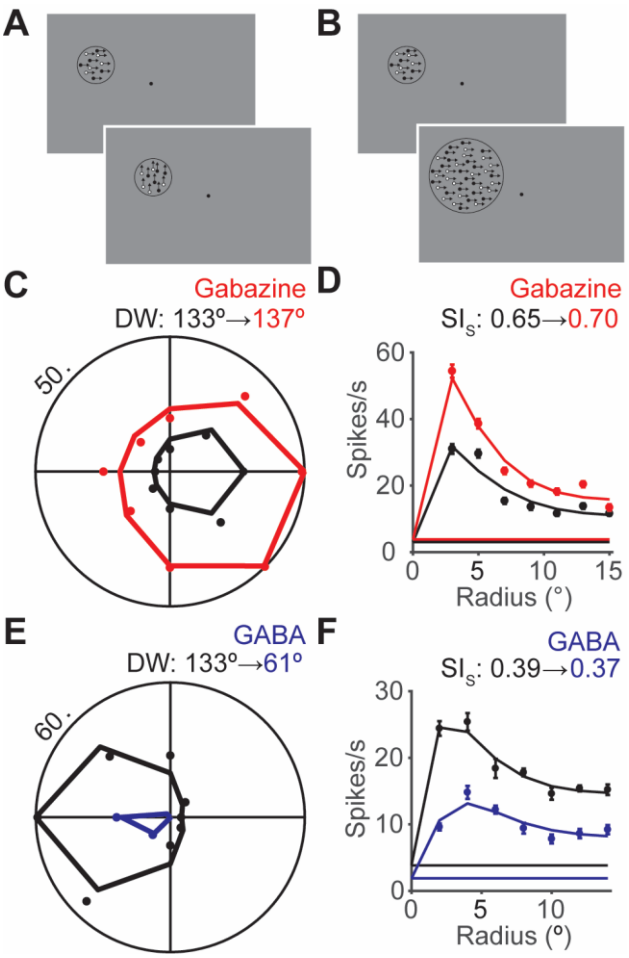

Figure 5. Effect of GABA on motion direction and size tuning. **A and B,** 100% coherent random dot patches were used to probe the direction and size tuning of MT neurons. **C and E,** Direction tuning curve for an example neuron before (black) and after injection of gabazine (C, red) or GABA (E, blue). The points are the mean responses for each direction. The lines indicate Gaussian function fits. Direction tuning width (DW) was defined as full width at half maximum of the fit. **D and F,** Size tuning curves for an example neuron, plotting the firing rate (mean ± s.e.m.) as a function of patch size before (black) and after injection of gabazine (D, red) or GABA (F, blue). The lines indicate difference of error functions fits. The horizontal lines show the spontaneous firing rate.

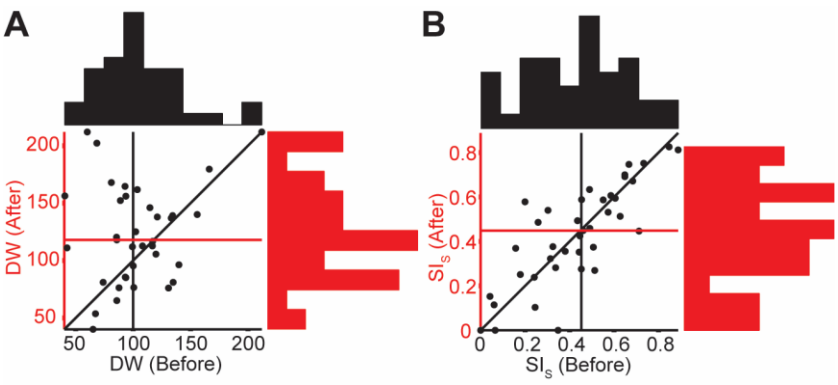

Figure 6. Population data on the effects of gabazine on direction and size tuning. **A,** Scatter plot of the direction tuning width before the injection of gabazine against the tuning width after injection (rank sum test, $p = 0.04$). Red and black lines represent the medians of the respective marginal distributions. **B,** Scatter plot of the neuronal size suppression index (SI_S) before the injection of gabazine against the neuronal SI_S after injection (rank sum test, $p = 0.98$).

Discussion

Through electrophysiological recordings in awake monkeys, we have found contrast-dependent surround suppression in MT in a space defined by motion directions. In addition, we found that local manipulation of the efficacy of GABAergic inhibition had little influence on standard measures of surround suppression. Both results are consistent with predictions of the stabilized supralinear network (SSN), previously tested in V1 (Rubin et al., 2015).

SSN as a unifying motif for normalization in multiple cortical areas

The contrast dependence of surround suppression in the space domain has been observed in both V1 and MT (Polat et al., 1998; Kapadia et al., 1999; Sceniak et al., 1999; Pack et al., 2005; Schwabe et al., 2010; Tsui and Pack, 2011). These results have previously been modeled under the assumption that inhibitory neurons have higher contrast thresholds than excitatory neurons (Somers et al., 1998; Huang et al., 2008; Schwabe et al., 2010; Carandini and Heeger, 2012). However, there is little experimental support for this assumption, and some data that contradict it (Contreras and Palmer, 2003; Song and Li, 2008).

In the SSN, the excitatory and inhibitory units can have the same properties (Rubin et al., 2015). Each unit has a power-law input/output function, but is stabilized by network inhibition (Ozeki et al., 2009; Ahmadian et al., 2013; Rubin et al., 2015). With low contrast inputs, the recurrent interactions within the network are weak, so neurons act relatively independently, summing their feedforward inputs and responding according to their transfer functions. With higher-contrast inputs, strong recurrent connections within the network provide contrast- and size-dependent suppression, with size in the spatial and feature (direction) domains playing similar roles.

552 The SSN also predicts that the local blockade of $GABA_A$ receptors should not reduce
553 surround suppression (Ozeki et al., 2009). In the SSN, surround suppression is not a result of an
554 increase in inhibitory GABAergic input, but a withdrawal of both excitation and inhibition. In
555 contrast, in models in which surround suppression results from an increase in the inhibition
556 received by suppressed neurons (e.g., Tsui and Pack, 2011), local blockade of inhibition should
557 reduce or prevent surround suppression.

558 Modulatory influences in visual cortex are often modeled within the normalization
559 framework, which is hypothesized to be a generic computation with equal validity across brain
560 regions and stimulus modalities (Carandini et al., 1997; Reynolds and Heeger, 2009; Carandini
561 and Heeger, 2012; Krause and Pack, 2014). The normalization model as typically conceived, is a
562 phenomenological rather than circuit model, in which some form of unnormalized neuronal
563 response is suppressed by the sum of unnormalized responses in other neurons that constitute the
564 "normalization pool". The precise form of normalization, for example whether the normalizing
565 pool constitutes all neurons or is restricted in some way based on neuronal tuning, must be
566 matched to fit the particular experiments modeled.

567 The SSN can be regarded as a circuit instantiation of the normalization model, in that
568 many SSN results closely match the results of an appropriately constructed normalization model
569 (Rubin et al., 2015). In the circuit implementation, the form of normalization is determined by
570 the connectivity. For example, in the SSN, orientation-specific long-range horizontal
571 connectivity leads to the orientation-selectivity of surround suppression (Rubin et al., 2015); in a
572 normalization model, this would be explained by assuming that the normalization pool consists
573 of neurons of similar preferred orientations to the normalized cell. The normalization model does
574 not explain the mechanism of suppression, and alternative mechanisms yield different

575 predictions. For example, if the normalization pool exerted suppression by adding inhibition to
576 the normalized cells, then one would expect increased inhibition and increased conductance in
577 normalized (e.g., surround-suppressed) cells, and local GABAergic blockade would reduce or
578 eliminate the normalization. In the SSN mechanism, normalization typically results from a
579 decrease in both excitation and inhibition and thus a decreased conductance (Rubin et al., 2015).
580

581 *Relationship to motion integration in MT*

582 In MT, the integration of different motion directions has frequently been probed with the plaid
583 stimuli (Movshon et al., 1985; Smith et al., 2005), comprised of superimposed gratings moving
584 in different directions. Previous work has distinguished between pattern cells, which respond to
585 the plaid motion direction, and component cells, which respond to the individual grating motion
586 directions (Movshon et al., 1985).

587 In the terminology used here, a plaid stimulus moving in a neuron's preferred direction
588 entails component motion confined to the directional surround. Thus for a high-contrast plaid,
589 the component gratings should suppress the neuron's response, and this could contribute to the
590 observed responses of component neurons. Furthermore, component-selective neurons have
591 small direction centers (i.e. narrow tuning width), so that they do not integrate input from two
592 gratings moving in very different directions (Rust et al., 2006; Tsui et al., 2010; Khawaja et al.,
593 2013).

594 Pattern cells have broader direction tuning than component cells (Rust et al., 2006;
595 Khawaja et al., 2013). Direction tuning, measured from the responses to individual motion
596 directions, corresponds to the "minimal response field" in visual space, the region in which small
597 stimuli can activate the cell; this measure does not change with contrast (Song and Li, 2008). Our

598 measure of motion integration is not correlated with direction tuning width (Fig. 4E), and is best
599 related to the "summation field size" in visual space, the size of a stimulus that best drives a cell
600 before further size increases cause surround suppression. The summation field size, like our
601 measure of motion integration, shrinks with contrast (Sceniak et al., 1999). We found a weak
602 correlation between our motion integration index and the pattern index, which quantifies
603 integration of plaid stimuli (Fig. 4D). These results suggest that the motion-domain summation
604 field and pattern selectivity are linked, but that summation on its own is insufficient to account
605 for pattern selectivity.

606 Pattern cells also show stronger suppression than component cells by stimuli moving
607 opposite to their preferred directions (Rust et al., 2006). This suggests a direction-domain
608 analogue of the "far surround" suppression that is found in the space domain; such suppression is
609 also regulated by contrast both in the direction domain in MT (Pack et al., 2005) and in spatial
610 surrounds in V1 (Schwabe et al., 2010). Our stimuli did not contain null-direction motion, and so
611 they would not have probed this component of the MT receptive fields. Nevertheless, an
612 inference from the existing data is that pattern cells in MT have both larger directional
613 summation fields and larger (or stronger) directional surrounds.

614 It can be argued that random-dot stimuli are larger than gratings in the direction domain,
615 as they activate a broader range of columns in V1 (Simoncelli and Heeger, 1998). Thus stimuli
616 composed of multiple dots fields moving in different directions might elicit stronger suppression
617 than grating stimuli containing a similar number of directions. Evidence in support of this idea
618 comes from studies that use transparent motion stimuli, comprised of overlapping dot fields
619 moving in two different directions. These stimuli evoke responses in MT that seem to reflect a
620 suppression of responses to stimuli that straddle the preferred direction (Xiao and Huang, 2015),

621 particularly for pattern cells (McDonald et al., 2014). One prediction of the current work is that
622 such suppression should be weaker for low-contrast stimuli.
623
624 *Functional correlates of integration and suppression*
625 A number of psychophysical studies have drawn a close link between contrast-dependent
626 responses in MT and visual motion perception. For simple motion discrimination tasks,
627 performance mirrors spatial processing in MT: for high-contrast stimuli, performance is worse
628 for large than for small stimuli (Tadin et al., 2003; Liu et al., 2016). Similarly, motion perception
629 can decrease at high contrasts when the stimulus speed is low, mirroring the contrast-dependent
630 suppression found in MT (Pack et al., 2005; Seitz et al., 2008). In the direction domain, MT
631 neurons exhibit higher null-direction suppression when the stimulus is high in contrast (Pack et
632 al., 2005). This suggests further that suppressive influences are stronger for high-contrast stimuli,
633 and there is some evidence that motion perception can worsen as the size of the stimulus
634 increases in the direction domain (Treue et al., 2000; Dakin et al., 2005). Conversely, motion
635 discrimination with noisy dots can sometimes improve at low contrast (Tadin et al., 2003). Our
636 results predict the ability to integrate motion signals in the direction domain should
637 systematically improve at low contrast, as has been found with manipulations of stimulus speed
638 (Seitz et al., 2008) and spatial size (Tadin et al., 2003).
639
640 *Conclusion*
641 A growing body of evidence points to a set of generic computations that are similar across brain
642 regions (Creutzfeldt, 1977; Barlow, 1985; Miller, 2016) and across sensory modalities
643 (Mountcastle, 1978; Pack and Bensmaia, 2015). Although this idea is attractive from a

theoretical standpoint, it remains somewhat speculative. In this work, we have provided an experimental test of the genericity of one computational model by comparing results in MT with those obtained previously in V1. The qualitative pattern of results is similar, supporting the possibility that this model provides a more general framework for modulatory responses and integration in cortex.

References

Ahmadian Y, Rubin DB, Miller KD (2013) Analysis of the stabilized supralinear network. Neural Comput 25:1994-2037.

Albright TD (1984) Direction and orientation selectivity of neurons in visual area MT of the macaque. J Neurophysiol 52:1106-1130.

Allman J, Miezin F, McGuinness E (1985) Stimulus specific responses from beyond the classical receptive field: neurophysiological mechanisms for local-global comparisons in visual neurons. Annu Rev Neurosci 8:407-430.

Angelucci A, Bullier J (2003) Reaching beyond the classical receptive field of V1 neurons: horizontal or feedback axons? J Physiol Paris 97:141-154.

Angelucci A, Bressloff PC (2006) Contribution of feedforward, lateral and feedback connections to the classical receptive field center and extra-classical receptive field surround of primate V1 neurons. Prog Brain Res 154:93-120.

Barlow HB (1985) The twelfth Bartlett memorial lecture: the role of single neurons in the psychology of perception. Q J Exp Psychol A 37:121-145.

Bolz J, Gilbert CD (1986) Generation of end-inhibition in the visual cortex via interlaminar connections. Nature 320:362-365.

Born RT, Tootell RB (1992) Segregation of global and local motion processing in primate middle temporal visual area. Nature 357:497-499.

Born RT, Bradley DC (2005) Structure and function of visual area MT. Annu Rev Neurosci 28:157-189.

Carandini M, Heeger DJ (2012) Normalization as a canonical neural computation. Nat Rev Neurosci 13:51-62.

673 Carandini M, Heeger DJ, Movshon JA (1997) Linearity and normalization in simple cells of the
674 macaque primary visual cortex. Journal of Neuroscience 17:8621.
675 Cavanaugh JR, Bair W, Movshon JA (2002) Nature and interaction of signals from the receptive
676 field center and surround in macaque V1 neurons. J Neurophysiol 88:2530-2546.
677 Chagnac-Amitai Y, Connors BW (1989) Horizontal spread of synchronized activity in neocortex
678 and its control by GABA-mediated inhibition. J Neurophysiol 61:747-758.
679 Contreras D, Palmer L (2003) Response to contrast of electrophysiologically defined cell classes
680 in primary visual cortex. J Neurosci 23:6936-6945.
681 Cossell L, Iacaruso MF, Muir DR, Houlton R, Sader EN, Ko H, Hofer SB, Mrsic-Flogel TD
682 (2015) Functional organization of excitatory synaptic strength in primary visual cortex. Nature
683 518:399-403.
684 Creutzfeldt OD (1977) Generality of the functional structure of the neocortex.
685 Naturwissenschaften 64:507-517.
686 Dakin SC, Mareschal I, Bex PJ (2005) Local and global limitations on direction integration
687 assessed using equivalent noise analysis. Vision Res 45:3027-3049.
688 DeAngelis GC, Uka T (2003) Coding of horizontal disparity and velocity by MT neurons in the
689 alert macaque. J Neurophysiol 89:1094-1111.
690 Huang X, Albright TD, Stoner GR (2008) Stimulus dependency and mechanisms of surround
691 modulation in cortical area MT. J Neurosci 28:13889-13906.
692 Hunter JN, Born RT (2011) Stimulus-dependent modulation of suppressive influences in MT. J
693 Neurosci 31:678-686.
694 Jones HE, Grieve KL, Wang W, Sillito AM (2001) Surround suppression in primate V1. J
695 Neurophysiol 86:2011-2028.

Kapadia MK, Westheimer G, Gilbert CD (1999) Dynamics of spatial summation in primary visual cortex of alert monkeys. Proc Natl Acad Sci U S A 96:12073-12078.

Khawaja FA, Liu LD, Pack CC (2013) Responses of MST neurons to plaid stimuli. J Neurophysiol 110:63-74.

Krause MR, Pack CC (2014) Contextual modulation and stimulus selectivity in extrastriate cortex. Vision Res 104:36-46.

Leventhal AG, Wang Y, Pu M, Zhou Y, Ma Y (2003) GABA and its agonists improved visual cortical function in senescent monkeys. Science 300:812-815.

Levitt JB, Lund JS (1997) Contrast dependence of contextual effects in primate visual cortex. Nature 387:73-76.

Liu LD, Pack CC (2017) The Contribution of Area MT to Visual Motion Perception Depends on Training. Neuron 95:436-446 e433.

Liu LD, Haefner RM, Pack CC (2016) A neural basis for the spatial suppression of visual motion perception. Elife 5.

McDonald JS, Clifford CW, Solomon SS, Chen SC, Solomon SG (2014) Integration and segregation of multiple motion signals by neurons in area MT of primate. J Neurophysiol 111:369-378.

Miller KD (2016) Canonical computations of cerebral cortex. Curr Opin Neurobiol 37:75-84.

Mountcastle VB (1978) Brain mechanisms for directed attention. J R Soc Med 71:14-28.

Movshon JA, Adelson EH, Gizzi MS, Newsome WT (1985) The analysis of visual moving patterns. In: Pattern Recognition Mechanisms (Chagas C, Gattass R, Gross C, eds), pp 117-151. New York: Springer.

718 Nealey TA, Maunsell JH (1994) Magnocellular and parvocellular contributions to the responses
719 of neurons in macaque striate cortex. J Neurosci 14:2069-2079.
720 Ozeki H, Finn IM, Schaffer ES, Miller KD, Ferster D (2009) Inhibitory stabilization of the
721 cortical network underlies visual surround suppression. Neuron 62:578-592.
722 Ozeki H, Sadakane O, Akasaki T, Naito T, Shimegi S, Sato H (2004) Relationship between
723 excitation and inhibition underlying size tuning and contextual response modulation in the cat
724 primary visual cortex. J Neurosci 24:1428-1438.
725 Pack CC, Bensmaia SJ (2015) Seeing and Feeling Motion: Canonical Computations in Vision
726 and Touch. PLoS Biol 13:e1002271.
727 Pack CC, Hunter JN, Born RT (2005) Contrast dependence of suppressive influences in cortical
728 area MT of alert macaque. J Neurophysiol 93:1809-1815.
729 Polat U, Mizobe K, Pettet MW, Kasamatsu T, Norcia AM (1998) Collinear stimuli regulate
730 visual responses depending on cell's contrast threshold. Nature 391:580-584.
731 Raiguel S, Van Hulle MM, Xiao DK, Marcar VL, Orban GA (1995) Shape and spatial
732 distribution of receptive fields and antagonistic motion surrounds in the middle temporal area
733 (V5) of the macaque. Eur J Neurosci 7:2064-2082.
734 Reynolds JH, Heeger DJ (2009) The normalization model of attention. Neuron 61:168-185.
735 Rubin DB, Van Hooser SD, Miller KD (2015) The stabilized supralinear network: a unifying
736 circuit motif underlying multi-input integration in sensory cortex. Neuron 85:402-417.
737 Rust NC, Mante V, Simoncelli EP, Movshon JA (2006) How MT cells analyze the motion of
738 visual patterns. Nat Neurosci 9:1421-1431.
739 Sceniak MP, Ringach DL, Hawken MJ, Shapley R (1999) Contrast's effect on spatial summation
740 by macaque V1 neurons. Nat Neurosci 2:733-739.

741 Schwabe L, Ichida JM, Shushruth S, Mangapathy P, Angelucci A (2010) Contrast-dependence of
742 surround suppression in Macaque V1: experimental testing of a recurrent network model.
743 Neuroimage 52:777-792.
744 Seitz AR, Pilly PK, Pack CC (2008) Interactions between contrast and spatial displacement in
745 visual motion processing. Curr Biol 18:R904-906.
746 Simoncelli EP, Heeger DJ (1998) A model of neuronal responses in visual area MT. Vision Res
747 38:743-761.
748 Smith MA, Majaj NJ, Movshon JA (2005) Dynamics of motion signaling by neurons in macaque
749 area MT. Nat Neurosci 8:220-228.
750 Snowden RJ, Treue S, Andersen RA (1992) The response of neurons in areas V1 and MT of the
751 alert rhesus monkey to moving random dot patterns. Exp Brain Res 88:389-400.
752 Somers DC, Todorov EV, Siapas AG, Toth LJ, Kim DS, Sur M (1998) A local circuit approach
753 to understanding integration of long-range inputs in primary visual cortex. Cereb Cortex 8:204-
754 217.
755 Song XM, Li CY (2008) Contrast-dependent and contrast-independent spatial summation of
756 primary visual cortical neurons of the cat. Cereb Cortex 18:331-336.
757 Tadin D, Lappin JS, Gilroy LA, Blake R (2003) Perceptual consequences of centre-surround
758 antagonism in visual motion processing. Nature 424:312-315.
759 Thiele A, Distler C, Korbmacher H, Hoffmann KP (2004) Contribution of inhibitory
760 mechanisms to direction selectivity and response normalization in macaque middle temporal
761 area. Proc Natl Acad Sci U S A 101:9810-9815.

762 Thiele A, Herrero JL, Distler C, Hoffmann KP (2012) Contribution of cholinergic and
763 GABAergic mechanisms to direction tuning, discriminability, response reliability, and neuronal
764 rate correlations in macaque middle temporal area. J Neurosci 32:16602-16615.
765 Treue S, Hol K, Rauber HJ (2000) Seeing multiple directions of motion-physiology and
766 psychophysics. Nat Neurosci 3:270-276.
767 Tsodyks MV, Skaggs WE, Sejnowski TJ, McNaughton BL (1997) Paradoxical effects of
768 external modulation of inhibitory interneurons. J Neurosci 17:4382-4388.
769 Tsui JM, Pack CC (2011) Contrast sensitivity of MT receptive field centers and surrounds. J
770 Neurophysiol 106:1888-1900.
771 Tsui JM, Hunter JN, Born RT, Pack CC (2010) The role of V1 surround suppression in MT
772 motion integration. J Neurophysiol 103:3123-3138.
773 Xiao J, Huang X (2015) Distributed and Dynamic Neural Encoding of Multiple Motion
774 Directions of Transparently Moving Stimuli in Cortical Area MT. J Neurosci 35:16180-16198.
775